# A new patterned air-flow device to reveal the network for tactile motion coding using fMRI

B. Nazarian, J. Caron-Guyon, J.L. Anton, J. Sein, J. Baurberg, N. Catz, Anne Kavounoudias

Version of Record: https://www.sciencedirect.com/science/article/pii/S0165027021003320
Manuscript_9d1601917f74c476fba15c84e5b9a24b

# A NEW PATTERNED AIR-FLOW DEVICE TO REVEAL THE NETWORK FOR TACTILE MOTION CODING USING FMRI

*Nazarian B[1¤], Caron-Guyon J[2¤], Anton JL[1], Sein J[1], Baurberg J[1], Catz N[2] & Kavounoudias A[2*]*

1. Aix Marseille Univ, CNRS, Centre IRM-INT@CERIMED (Institut des Neurosciences de la Timone – UMR 7289), Marseille, France

2. Aix Marseille Univ, CNRS, LNC (Laboratoire de Neurosciences Cognitives – UMR 7291), Marseille, France

¤ First co-authors: Nazarian B & Caron-Guyon J have equally contributed to this work

* Corresponding author : Anne.Kavounoudias@univ-amu.fr

## HIGHLIGHTS

- The PAF can deliver stable and reliable complex airflow patterns
- The device is easy-to-set-up and fully fMRI compliant
- Psychophysical tests show that it can be used to discriminate airflow directions
- Different tactile patterns could be decoded by fMRI measurements
- It is useful for studying complex tactile motion coding/perception

## ABSTRACT

**Background**

Studying brain processes underlying tactile perception induced by natural-like stimulation is challenging yet crucial to closely match real-world situations.

**New Method**

We developed a computer-controlled pneumatic device that allows the delivery of complex airflow patterns on subject's body, through a MR-compatible system fixed on an independent clippable mounting device. The intensity of stimulation as well as the timing of each of the four air channels are completely programmable and independent, allowing the precise control and modularity of the airflow delivery.

**Results**

An analysis of signal-to-noise ratio (SNR) measurement did not show any impact of the PAF device on anatomical or functional scan acquisitions. A psychophysical experiment was also performed on 24 volunteers to evaluate the perception of different airflow patterns delivered over the lower part of their face. It revealed that all participants were able to finely discriminate the direction of these leftward to rightward flow motions. The fMRI experiment, which consisted in presenting to 20 participants four different airflow patterns, shed light on the brain network associated with tactile motion perception. A multivariate analysis further showed a specific coding of the different patterns inside this tactile brain network including the primary and secondary somatosensory cortex

**Comparison with Existing Method(s)**

The Patterned Air-Flow (PAF) is an easy-to-set-up, portable, adaptable device, which can be spatially and temporally modulated to provide complex tactile stimuli.

**Conclusions**

This device will be useful to further explore complex dynamic touch exerted over various body parts and can also be combined with visual or auditory stimulation to study multisensory mechanisms.

**Keywords: air stimulation, pneumatic device, motion perception, cerebral network, MVPA**

## 1. INTRODUCTION

While visual motion has been extensively studied, motion perception in the other sensory modalities have received less attention, especially in the tactile domain. Functional MRI experiments come with the major limitation of requiring devices compatible with the scanner environment. Generating a tactile motion percept, with computer-controlled stimuli, in the fMRI scanner has been made possible by several devices including piezoelectrical stimulations or braille-like dot patterns delivered on the finger pulp (Debowska et al., 2013; Ricciardi et al., 2007; Sani et al., 2010; Summers et al., 2009; Van Kemenade et al., 2014; Wacker et al., 2011; Puckett et al. 2017), probes moving towards or away from the participant's egocentre on their finger (Amemiya et al., 2017), and even the presentation of real moving physical objects on subjects' hands or fingers (Basso et al., 2012; Blake et al., 2004; Landelle et al., 2020). Another type of somatosensory set-up which has recently been developed and used in multiple studies investigating somatosensory processing, especially somatotopy, uses pneumatics devices (Hao et al., 2013; Huang and Sereno, 2007; Zappe et al., 2004). Huang and Sereno (2007) have for instance developed a system, called the Dodecapus, that can be mounted on the head coil and that can deliver point somatosensory stimulation across the participant's face, which allowed a precise description of the somatosensory face map in the parietal cortex.

However, the ability to perceive complex dynamic airflow stimulation and its neural basis have received less attention so far, while in the visual domain, optic flows have been extensively used to study self-motion processing (Arnoldussen et al., 2011; Indovina et al., 2013; Kleinschmidt et al., 2002; Kovacs et al., 2008). Creating a tactile stimulation resembling perceptually what optic flow fields produce is therefore pivotal to improve our understanding of tactile motion perception, in ecologically-valid contexts. The generation of spatially-oriented airflow across the face is made possible by the device developed and presented in this article.

Here we describe the design and experimental evaluation of an innovative MR-compatible stimulator enabling precise and reproducible delivery of static or dynamic patterns of airflows. Indeed, the p*atterned airflow* (PAF) device enables the precise control of air pressure in each of four pneumatic channels, allowing the

customization of airflows by modulating independently each air nozzle. It can thus be used to create airflows across the participants' face, and modulated to produce radial or translational tactile motion with different flow rates and patterns. It is fully controlled by a dedicated software implemented in the Labview environment that enables the generation of spatial and temporal complex patterns. The PAF device can therefore generate controlled airflows with a predefined orientation, moving laterally or horizontally according to the arrangement of the nozzles, or even randomly stimulating different parts of the body like the face at different levels of pressure intensity.

We present here technical and experimental tests performed to validate the present device as an MR-compatible tool useful to study tactile motion perception and its neural basis. First, we verified that this device did not affect anatomical or functional images acquired with a 3T MR scanner. In addition, a psychophysical study was carried out on 24 adult volunteers to assess whether, when applied over the face, different airflow patterns can be discriminated, meaning that this device is fine enough to study complex tactile motion perception. Finally, we examined whether different patterns of tactile stimulation resulted in various brain activations evidenced by an fMRI experiment performed on 20 adults. In particular, using a multivariate pattern analysis (MVPA) approach, we explored whether various tactile patterns were differently coded within specific regions of the somatosensory network. If satisfied, such tests and analyses will validate this new device as a promising tool to investigate tactile motion perception and the neural basis of complex natural-like airflow.

## 2. MATERIAL AND METHODS

### *2.1. The Patterned Air-Flow device (PAF): design and control*

The airflow stimulator is composed of a three-stage circuit (Fig. 1A): an air pressure regulation stage, a stage for distributing and monitoring the airflow, and a peripheral stimulation stage. The airflow stimulator is based on the use of proportional control valves solenoids (SMC PVQ30) allowing the precise control of the valves' opening levels by driving a variable current in the solenoid. Thus, given a constant input pressure, the solenoid valve allows the control of the airflow's intensity. The stimulator is connected to a medical air source,

which has a minimum 5 bars pressure. A pressure regulator (SMC ITV1030) is controlled by an analog voltage input and ensures a constant 2 bars pressure at the input of all the valves (an analog output of the ITV1030 allows to control the actual pressure at any time ; Fig. 1A). According to this constant inflow pressure, the downstream airflow is modulated only by the valve opening, i.e. the driving current. As most of the analog I/O cards can only generate variable voltage outputs, we built a specific electronic board to convert a voltage output into a regulated current driving (Fig. 1B). Each electro-valve output is connected to a flowmeter (Key Instruments MR3A17BVBN; Fig. 1A middle part) that allows the precise calibration of each pneumatic channel.

The pneumatics are controlled using a specific software interface written using the National Instruments LabVIEW © 2017 environment. The program is driving two multifunction National Instruments cards : 1) a PXI-6289 with 4 analog voltage outputs, dedicated to drive the proportional electro-valve' openings, 2) a USB-6002 dedicated to the pressure regulator : an analog voltage output sends the command to the regulator while an analog input allows to control the effective pressure given by the regulator.

The online supervision of each pneumatic channel was enabled by the development of a supervising interface written on LabVIEW © 2017 (as shown in Fig. 2). The colored sliders indicate the flow level in each of the pneumatic channels. The inflow pressure is also displayed online, allowing its monitoring and preventing any pressure loss.

The airflow controller (Fig.1A & 1B) was placed outside the scanner room, leaving no possibility for any interactions with the electronic system. Only the tubes (Fig.1C) were going inside the room and MRI scanner, through waveguide tubes.

The system can be modulated to fit the requirements of numerous experimental designs. In this study, we only tested a few ways to use the airflow stimulator, to investigate the resulting perception and the corresponding neural processing.

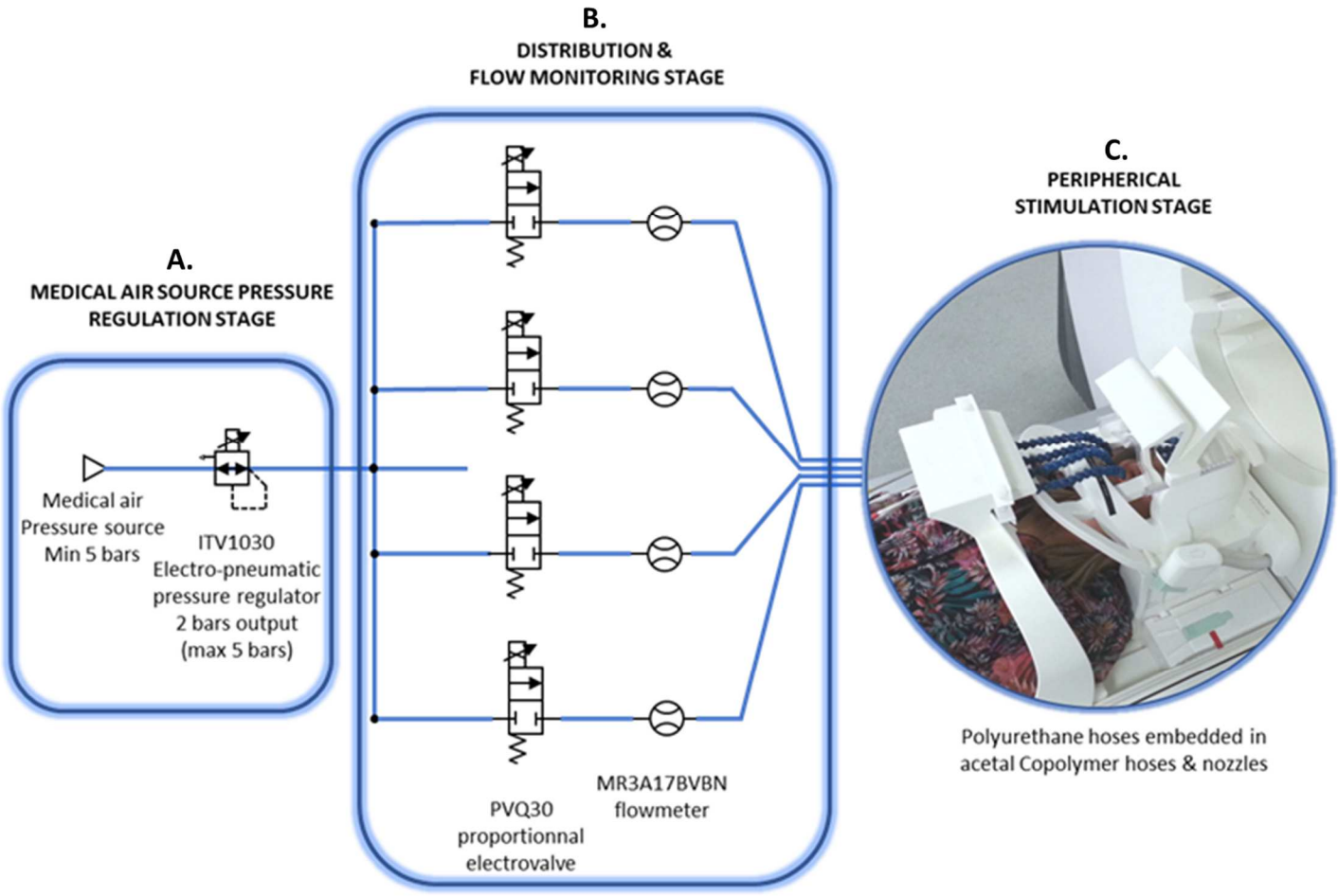


**Figure 1. Schematic representation of the pneumatic components of the PAF device**

Pneumatic circuit diagram including three-stage circuit : A) pressure regulation stage in which the medical air source, which has a maximal pressure of 5 bars, is regulated by an electropneumatic pressure regulator which ensures the distribution of 2 bars to each downstream electrovalves, B) The flow distribution is modulated by proportional electrovalves and monitored using flowmeters, C) the air is transported via polyurethane hoses that are embedded in acetal copolymer hoses (blue) and nozzles (yellow), to reach the participant's body (in this study : the participant's face).

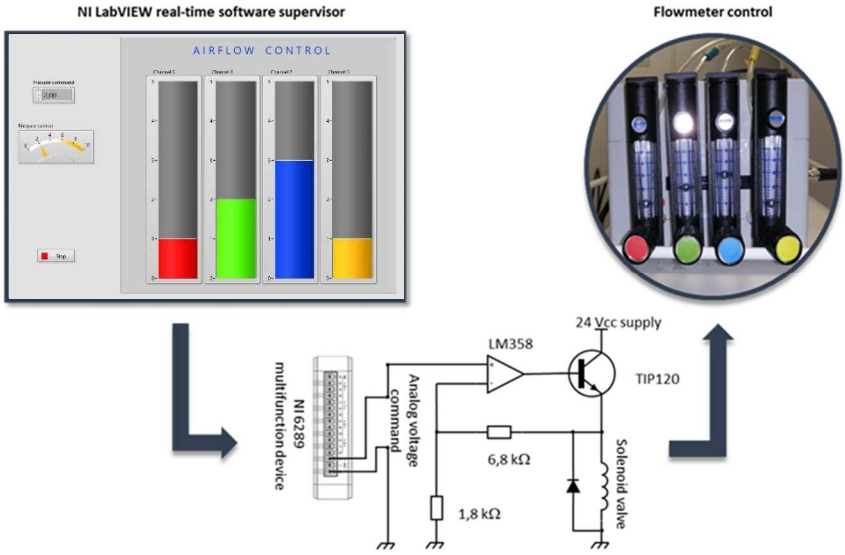


**Figure 2. Overview of the control on the PAF device**

A real-time software supervisor, written on LabVIEW © 2017, allows the online monitoring of the four pneumatic channels and control of the global airflow input rate. The solenoid valve opening is controlled using a specific electronic circuit converting the analog variable output voltage from the NI 6289 to a variable current that modulates the valve opening. A flowmeter device allows the visual control of the flow rates in each channel.

### *2.2 System set-up*

Participants were lying in the MRI scanner in the usual supine position. Inflatable cushions were inserted in the head coil on both sides of the subjects' head to improve participants' comfort while minimizing head movements.

The patterned airflow stimulator was fixed on a separate mounting device (Fig. 1) that was easy to set-up using a clip-on system to fix it on the MRI bed, after the installation of the participant. The input pressure was fixed to 2 bars (in order to match with the given calibration curves (current / opening) of the valves) for all participants, and the four nozzles were adjusted to stimulate four specific locations on the face when delivered separately (from the extreme left to the extreme right of the lower face under the participant's mouth). The inclination of the air puffs on the participants' face made it possible to generate sensations of airflow over the lower part of the face of various direction in the frontal plane.

For the psychophysical experiment, the environment was reproduced to create similar experimental context. The participants were lying on a bed with earplugs to mask the airflow noise and the system mounted on the bed.

### *2.3 Stimulations*

Tactile flow was created by using spatial patterns of air pressure in the four pneumatic channels, to produce global airflow stimulations (Fig. 3). Three flow levels were defined (Level 1 = 10 l/min, Level 2 = 20 l/min, Level 3 = 30 l/min) and precisely controlled for each pneumatic channel that were individually calibrated beforehand. For instance, the LeftMost airflow direction consisted in having the air nozzle 1 (the LeftMost) to the highest flow-rate (Lvl 3), air nozzle 2 to the middle flow-rate (Lvl 2), and air nozzles 3 and 4 to the lowest flow-rate (Lvl 1).

For the psychophysical experiment, we defined 5 flow spatial patterns using this modulation procedure, including two leftward (LeftMost and LeftMin), two rightward (RightMost and RightMin) and one *straight ahead* direction (Reference) (Fig. 3B).

For the fMRI experiment, 4 tactile conditions consisting in a combination of airflow spatial patterns varying in time were randomly presented: *left, right, flicker, motion*, presented for 8 seconds each and repeated 10 times. To create a rightward motion sensation, the highest flow-rate was sequentially assigned to the air nozzles from left to right with a time step of 0.4 s, while lower flow-rates were attributed to the other air nozzles to create the flow patterns (as depicted in Fig. 3B). A rightward motion thus consists in a 1.6 s-duration sequence of a successive Pattern 1 - Pattern 2 - Pattern 4 - Pattern 5, repeated five times in a row; the leftward motion consisted of the exact inverse sequence from Pattern 5 to Pattern 1. The *flicker* condition consisted of a very short activation (0.7 ms) of the air nozzles one by one in a random fashion yielding a sensation of random point activation with no coherent motion information. The *motion* condition consisted of having all the pneumatic channels activated simultaneously with waves of four increasing-decreasing flow levels (sequence

Lvl1-Lvl2-Lvl3-Lvl2-Lvl1), producing a sensation of global airflow moving towards and away from the center of the face.

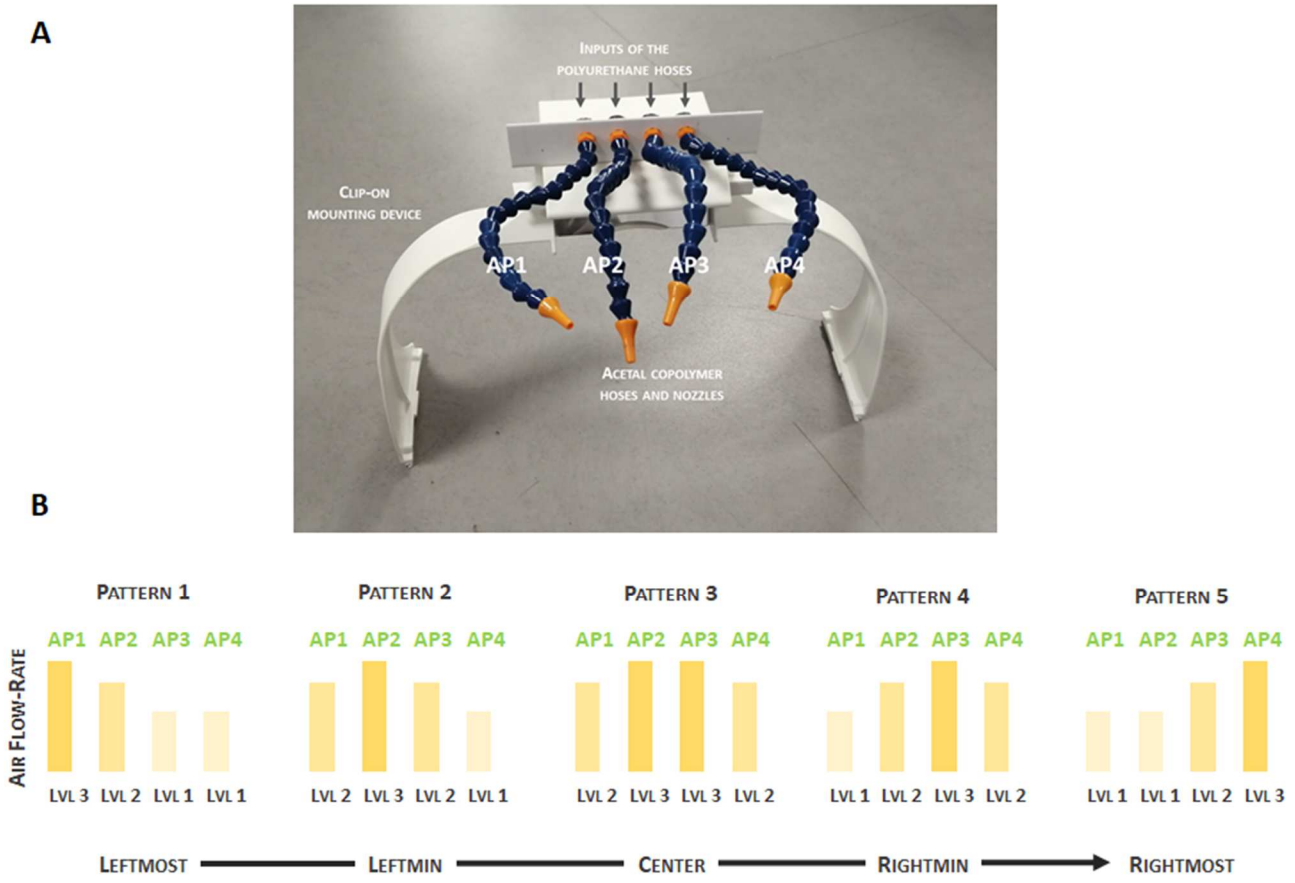


**Figure 3. The Airflow device and example of airflow spatial patterns.**

**A.** Air flow stimulator mounting device. The polyurethane hoses are plugged onto the acetal copolymer hoses (blue component) and nozzles (orange component) and constitute four air puffs (AP). This part of the setup is fixed onto a mounting device (white) that can be clipped-on the MRI scanner's bed. **B.** Three flow levels were defined (LVL1, LVL2, LVL3) and each of the four air puffs (AP1, AP2, AP3, AP4) were individually calibrated. Each pattern was created to produce different global flow directions. The five patterns correspond to the five directions of the psychophysical experiment (from leftmost to rightmost). The fMRI run used different temporal sequences of these patterns.

### *2.4 Participants*

Twenty-four participants (23.3 +/- 2.6 years old) were included in the psychophysical experiment, and 20 participants underwent the fMRI experiment (25.3 +/- 2.7 years old). All participants gave their written informed consent and the study in accordance with the Declaration of Helsinki was approved by the local ethics committee (CCP Marseille Sud 1 #RCB 2010-A00359-30).

### *2.5 Experimental Designs*

#### *2.5.1 Psychophysical experiment*

Tactile stimulations were presented in pairs, one direction being always presented with the reference direction (the *straight ahead* direction). The subjects had to perform two tasks : 1) determine whether the second stimulus was going more to the right or to the left as compared to the first stimulus, using the left- or right-click of the trackball mouse, and 2) describe the absolute direction of the second stimulus using the trackball which displayed an oblique line to be moved to match the perceived direction, sampled on a scale ranging from -10 to +10 (-10 = -54°; +10 = + 54°).

#### *2.5.2 fMRI experiment*

One functional session was carried out during brain activity recording. The tactile run consisted in 4 conditions (Motion, Flicker, Left, Right) randomly presented and lasted 8 seconds. To maintain the attentional level of the participants throughout this functional run, they were asked to detect a specific target stimulus. The target stimulus was a repetition of four fast alternating leftward and rightward airflows lasting 2.4 seconds. When participants detected this tactile target, they were asked to say 'Top'.

### *2.6 Image Acquisition*

3-Tesla Siemens Prisma MRI Scanner (Siemens, Erlangen, Germany) with the in-built body-coil for radiofrequency excitation and the manufacturer's 64- channel phased-array head coils for reception was used for the data acquisition. Functional Blood-oxygen Level Dependent (BOLD) images were acquired with a multiband sequence (Multi-Band EPI C2P R016a, provided by the University of Minnesota: Feinberg et al. 2010; Moeller et al. 2010; Xu et al. 2013). The MRI scanning began with the acquisition of a pair of whole-brain Spin-echo EPI images (TR/TE = 7060/59 ms, voxel size = 2.5 x 2.5 x 2.5 mm3, slices = 54, FOV (Field of View) = 210 x 210 mm2, flip angle = 90/180°) with opposite phase encoding polarities along the anterior-posterior axis., matching the geometry and the echo spacing as the BOLD images. These images will be used during pre-

processing stage for distortion correction of the BOLD images (see below). The BOLD images were then acquired using a gradient-echo EPI sequence (TR = 1224 ms, TE = 30 ms, flip angle = 65°, voxel size = 2.5 x 2.5 x 2.5 mm3, multiband factor = 3, 54 slices, FOV = 256 x 256 x 204.8 mm3). A total of 355 brain volumes were acquired during the functional tactile run.

Finally, a high-resolution T1-weighted (T1w) anatomical image was acquired (MPRAGE sequence: TR/TI/TE = 2400/1010/2.28 ms, flip angle = 8°, voxel size = 1 x 1 x 1 mm3, 256 slices, FOV = 256 x 256 x 204.8 mm3).

### *2.7 Image Analysis*

All acquired MR images in DICOM format were converted into nifti format and stored following the Brain Imaging Data Structure (BIDS) standard (http://bids.neuroimaging.io, Gorgolewski et al. 2016).

For each participant, the images were pre-processed using the fMRIprep procedure (RRID:SCR_016216 ; Esteban et al., 2019, available here : 10.5281/zenodo.852659) which is a Nipype-based tool (RRID:SCR_002502; Gorgolewski et al., 2011, available here : 10.5281/zenodo.581704.). This procedure includes a step of segmentation of brain tissue into cerebrospinal fluid (CSF), white matter (WM) and grey matter (GM) performed on the brain-extracted T1-weighted (FSL v5.0.9, RRID:SCR_002823). Functional images were (1) corrected for magnetic field inhomogeneities using a B0-nonuniformity map (or fieldmap) estimated based on the two echo-planar imaging (EPI) references with opposing phase-encoding directions, with 3dQwarp Cox and Hyde (1997) (AFNI 20160207) (2) realigned to correct for head movements between scans, (3) coregistered to the respective anatomical scan (4) normalized to the ICBM 152 Nonlinear Asymmetrical template version 2009c (RRID:SCR_008796, Fonov et al., 2009) (5) and smoothed with an isotropic three-dimensional Gaussian kernel of 6 mm.

For the functional session, task-dependent changes in the BOLD signal for each subject were modelled as boxcar regressors time-locked to the onsets of the stimulation conditions and convolved with the hemodynamic response function (HRF) of SPM12 (https://www.fil.ion.ucl.ac.uk/spm/). First level of contrasts

were then computed corresponding to all conditions tested: i.e. Left, Right, Flicker, Motion and Target conditions. To account for the nuisance of head motion on the BOLD signal, head movement parameters estimated by the motion realignment procedure were also included in the GLM as covariates of no interest using a 24-parameter autoregressive model of motion (Friston et al. 1996). We mitigated the physiological and other noise components of the fMRI data using aCompCor (Behzadi et al., 2007), which estimates the nuisance signals of tissues that are not expected to exhibit BOLD fMRI signals of neuronal origin, i.e. white matter and CSF, and includes the mean and the 12 principal components of the signal of those tissues in the GLM as additional regressors. The first-level contrast maps of the 20 participants were then entered into a second-level analysis to perform between-subject analysis.

A multivariate pattern analysis (MVPA) on all participants was also performed using Nilearn (Abraham et al., 2014, https://nilearn.github.io/), a python module. The pre-processed functional data were modeled to yield one beta per trial for the four conditions of interest (Motion, Flicker, Left, Right), while the non-interest conditions as well as the movement regressors were modeled as 1 beta for the whole run. For each participant, the region-of-interest (ROI) classification procedure was performed using a four-class support vector machine classifier, in a leave-one-trial-out procedure. The latter was indeed trained on 90% of the trials (9/10) to discriminate between the four tactile conditions (Motion, Flicker, Left, Right) and tested on the remaining 10% of the trials (1/10), yielding 10 cross-validations folds. This MVPA procedure was performed in anatomically-defined ROIs (SI, SII, IPL, SPL, V1) using the SPM Anatomy toolbox.

## 3. RESULTS - DISCUSSION

### *3.1 Psychophysical experiment*

The psychophysical experiment revealed that using patterns of airflow enabled the modulation of task difficulty (Fig. 4). Different airflow patterns allowed the participants to perceive different directions. Using the trackball values reported by the participants, we tested the ordering of the flows' directions (from to left to right) with a non-parametric Jonckheere-Terpstra trend test (Cardillo, 2021). This analysis revealed that

participants were able to correctly order the five directions of tactile airflow delivered to their face from the leftmost to the rightmost stimulation (Fig.4A; $U = 5224.5$; $JT = 10.865$; $p < 0.0001$). To analyze and depict the tactile performance, we also computed the classical psychometric curves i.e., the individual proportion of "more right oriented than the reference" answers fitted by a cumulative Gaussian function (Landelle et al. 2018). These psychometric curves are classically used to assess individual discrimination threshold (or just noticeable difference: JND) corresponding to the minimal difference in stimuli direction required to perceived a significant change. JND corresponds to the half of the direction stimuli difference between 25% and 75% of good answers. As the exact angle direction of the airflow stimuli could not be estimated, the discriminative thresholds were therefore estimated in arbitrary units (from 1 to 5) considering that stimulation were equidistant (Fig. 4B). With such units, the tactile discrimination threshold $JND_T$ at the group level was 0.74 ± 0.14 a.u.

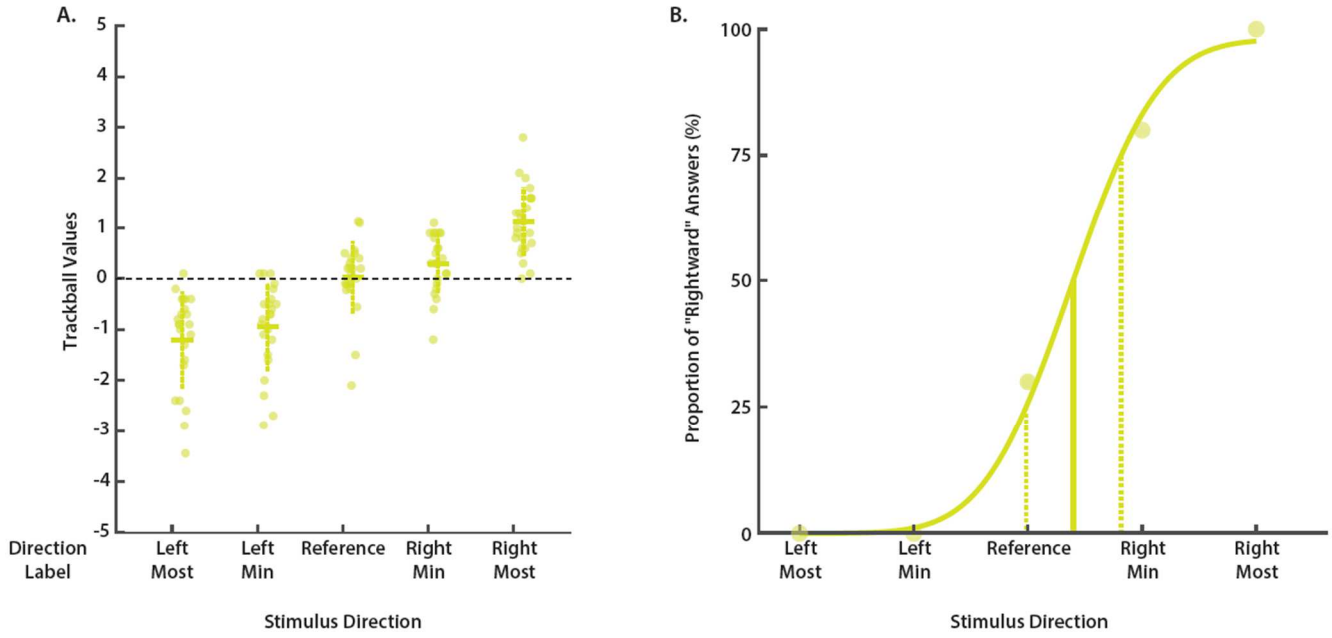


**Figure 4. Behavioral results on the perception of direction of the airflow stimuli.**

**A.** Mean trackball responses for the LeftMost to the RightMost tactile stimuli. For each direction of stimulation, the mean trackball response per participant (one circle represents one participant's mean value) is plotted using a scale range from -10 to +10 (1 unit = 5.4°). **B.** Tactile psychophysical curve for one subject. Proportions of "right" answers are plotted as a function of the stimulus' direction from LeftMost (1 a.u.) to RighMost (5 a.u.). Perpendicular dashed lines represent the intensities corresponding to the 25% and 75% thresholds extracted to compute the discrimination threshold (JND).

The present psychophysical results validate the possibility to estimate fine perception of motion direction using the PAF device.

### *3.2 fMRI tests*

#### *3.2.1 Effect of the PAF device on MR images*

RF noise measurement provided by the MRI manufacturer and separate analysis of SNR measurement on a water MRI phantom placed in the head coil did not show any impact of the device on the MR measurement. Images for the SNR measurements were acquired on the phantom with the same MPRAGE and EPI sequences applied for participants' acquisition: with and without the device being installed near the head coil (similar to the in vivo experiment). As shown in Fig. 5, we did not detect any artifacts created by the presence of the PAF device on the MPRAGE or EPI images of the phantom. We further computed noise measurement by acquiring signal from the reception chain without any excitation provide to the sample. No difference was observed with the noise measurement for the two conditions, with or without the presence of the device (data not shown). It is worth noting that this noise measurement is routinely used in our MRI Center before installing any new stimulation device and it was shown to be extremely sensitive to any kind of RF contamination around the Larmor frequency range. For SNR measurements, MRIQC software was used (Esteban et al. 2017). MRIQC provides a wide range of calibrated metrics to assess the quality of human brain images. In this case, we chose the "SNR total" metrics to evaluate the impact of the presence of the airflow device. A digression of 3.2% (SNR=77.1 without and SNR=74.6 with the device installed) and 2.3 % (SNR = 2.3067 without and SNR=2.3014 with the device installed) were observed on the MPRAGE and EPI scans, respectively. These digression values are within the standard variation of this measurement (Cheng et al. 2020; Yang et al. 2011) and show that the presence of the airflow device does not affect the MRI signal.

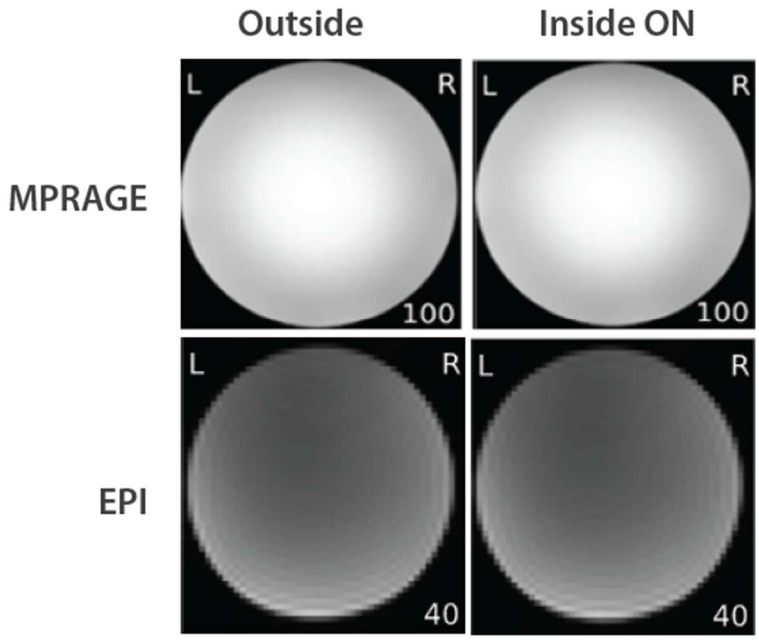


**Figure 5.** Visualization of one slice of the MPRAGE (top row) and EPI (bottom row) sequences when the device is out of the room (left column) and in close proximity of the headcoil and in function (right column) did not reveal any impact of the presence of the PAF device.

*3.2.1 Effect of the PAF device on head movements*

The effect of the PAF device on head movements was checked by plotting the head movements in the 6 directions and the framewise displacement (FD) for all participants (N=20), calculated with fMRIprep (Fig. 6). Airflow delivered by the PAF did not systematically induce head movements as demonstrated by the absence of modulation of the FD or any of the mean traces corresponding to the six directions in translation and rotation following the stimulation onsets throughout the run.

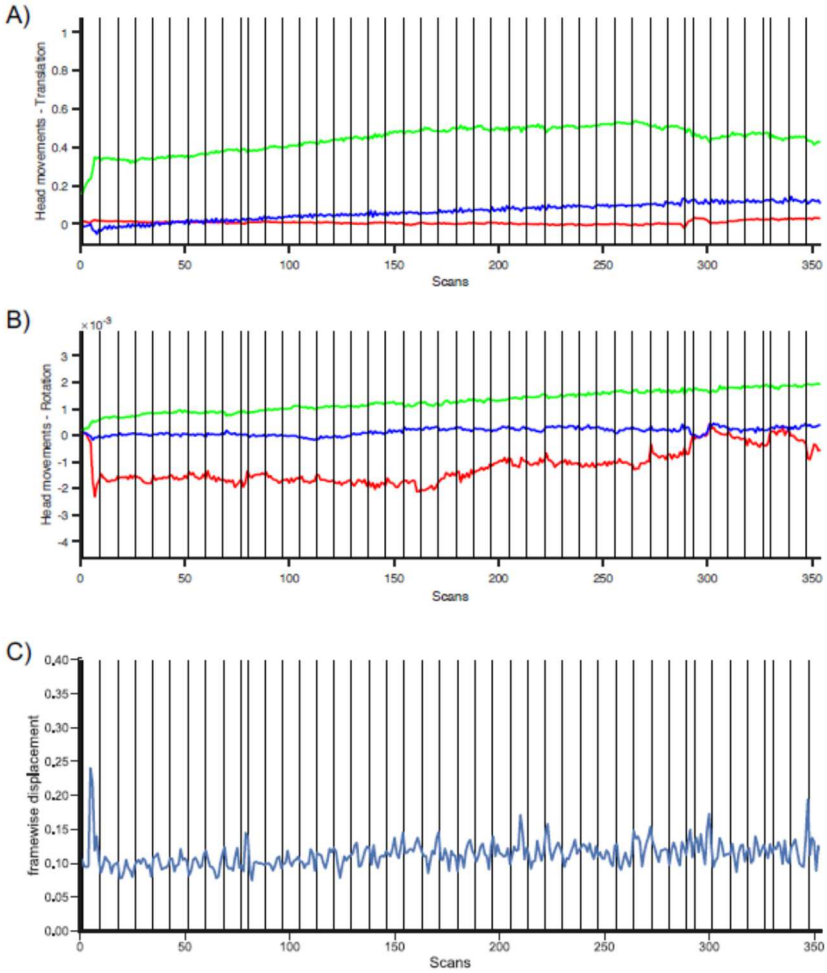


**Figure 6. Head movements and onsets of puff stimuli. A-B**. Colored lines represent the mean head movements, over the 20 participants, in the translational components (in mm) (**A**) and rotational components (in rad) (**B**) for the three directions (x: green; y: blue; z: red). **C**. Mean framewise displacement (FD in mm) calculated by FMRIPREP over all 20 participants. Each vertical line corresponds to the onset of a puff stimulus (Left, Right, Flicker, Motion or Target)

### *3.2.2 Bold signal changes induced by patterned airflow stimuli*

Univariate group analysis showed that compared to a no-motion condition (Flicker), the motion airflow condition activated more specifically a large bilateral somatosensory network including the primary somatosensory cortex (S1), secondary somatosensory cortex (SII), anterior insula, inferior frontal gyrus (IFG) and cerebellum, as well as the left anterior cingulate cortex (ACC) and putamen (Table 1, Fig. 7). The locations of activation within SI (left and right x/y/z peak coordinates in MNI space : -49/-20/41; 42/-18/41) were very

close to that already reported by Huang and Sereno (2007) (-51/-17/45; +52/-11/42), who also used an airflow device to apply punctuate stimulations on the face and Moulton et al. (2009) (left peak coordinates in MNI space for n=12 subjects: -61/-12/35), who applied brush-like stimuli to different parts of the face. It slightly differed from that reported by Dresel et al. (2008) (left and right x/y/z peak coordinates in MNI space for one subject: -56/-16/52; 60/-12/32) who used point-like stimuli on the face with Von Frey filaments, which are known to stimulate another kind of skin mechanoreceptors. By contrasting different patterns of airflow stimulation delivered by the present PAF device, this study shows that it is possible to reveal tactile motion brain network.

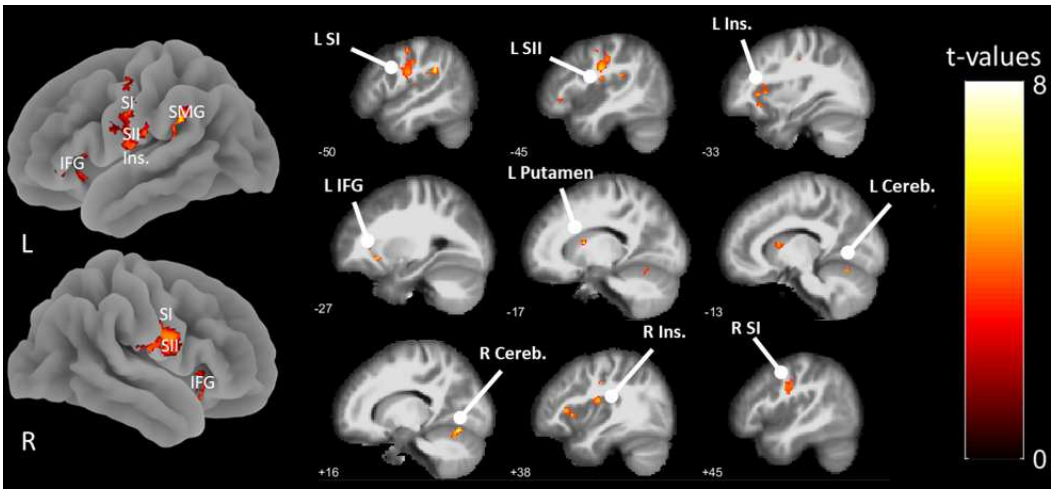


**Figure 7. Brain regions more activated during the Tactile Motion versus Static conditions (Tactile Motion > Flicker)**. Cortical statistical map ($p < 0.05$ FWE cluster corrected) obtained in the group-analysis is overlaid on inflated brain cortical surface and sagittal slices of a mean normalized anatomical image (x coordinates in MNI space). *L: left hemisphere, R: right hemisphere, Cereb: cerebellum, IFG: inferior frontal gyrus, INS: Insula, SI: primary somatosensory area, SII: secondary somatosensory area, SMG: SupraMarginal Gyrus.*

**Table 1. Group analysis of brain activations during airflow stimulation.**

| Regions | Extent | t-value | x | y | z |
|---|---|---|---|---|---|
| **Tactile Motion > Flicker** | | | | | |
| L Postcentral Gyrus | 806 | 6.084 | -49 | -11 | 22 |
| L Rolandic Operculum (SII) | | 4.253 | -44 | -12 | 20 |
| L Postcentral Gyrus (SI) | | 5.204 | -45 | -20 | 41 |
| R Rolandic Operculum (SII) | 575 | 6.883 | 40 | -9 | 18 |
| R Postcentral Gyrus (SI) | | 4.258 | 42 | -18 | 41 |
| L Inferior Parietal Lobule (SMG) | 161 | 7.126 | -51 | -43 | 30 |
| R Superior Temporal Gyrus | 44 | 4.783 | 58 | -27 | -1 |
| L Anterior Cingulate Cortex | 41 | 5.591 | -7 | 12 | 36 |
| L Posterior-Medial Frontal | 45 | 4.914 | -3 | -3 | 64 |
| R Inferior Frontal Gyrus (p. Orbitalis) | 48 | 7.375 | 46 | 20 | -9 |
| L Inferior Frontal Gyrus (p. Orbitalis) | 58 | 6.076 | -27 | 22 | -9 |
| R Insula Lobe | 114 | 6.118 | 38 | 20 | 2 |
| L Insula Lobe | 135 | 4.717 | -33 | 18 | 4 |
| L Putamen | 72 | 6.831 | -17 | 6 | 12 |
| R Cerebelum (VI) | 151 | 7.646 | 16 | -69 | -17 |
| L Cerebelum (VI) | 82 | 5.768 | -13 | -65 | -19 |

*MNI coordinates (x, y, z in mm) and t values refer to peaks of statistically significant activation in the left (L) and right (R) brain hemispheres (random effect analysis, N= 20 subjects), after correction for multiple comparison at the cluster level (FWE $p < 0.05$). SMG: supramarginal gyrus*

Furthermore, the MVPA analysis performed in anatomically-defined ROIs revealed that the four different patterns of airflow stimulation tested here (Right, Left, Flicker and Motion conditions) could be decoded above the level of chance (25%) in SI, SII, the IPL and SPL in both hemispheres (Fig. 8). On the other hand, these four motion classes could not be significantly decoded above-chance at the group-level in the primary visual area (V1). This decoding approach reveals how motion patterns produced by the PAF system are sufficiently subtle and reproducible to produce distinct and stable cerebral patterns in the tactile processing network.

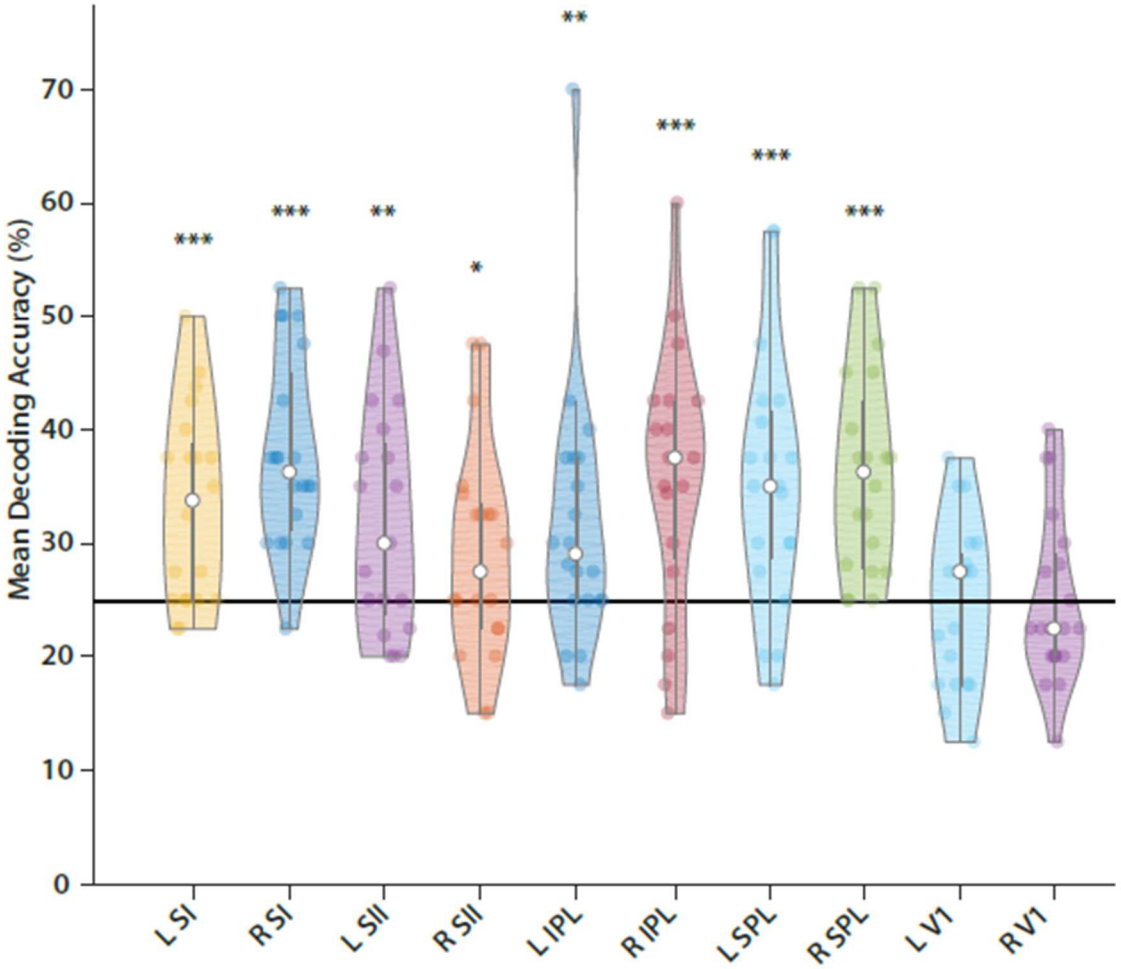


**Figure 8. Group-level anatomical Region-of-Interest tactile decoding analysis.**

Violin plots represent the decoding accuracy of the four classes of tactile motion (Motion, Flicker, Left, Right) computed for 5 regions of interests (SI, SII, IPL, SPL, V1) in both hemispheres (L, R) for all participants. The horizontal black line represents the chance level (25%). Colored circles represent individual decoding accuracy, white circles and vertical black lines represent the population's median and standard deviation respectively. A right-tailed Wilcoxon signed rank test against chance level (25%) was performed. * : $p < 0.05$, ** : $p < 0.01$, *** : $p < 0.001$.

## 4. CONCLUSION

In this study, a MR-compatible airflow stimulator was developed and tested in a psychophysical and an fMRI experiment. The different technical verifications confirmed that the PAF system does not induce any noise or distortions in the MR images acquired. In addition, no head movement was triggered by the airflow, thus eliminating the critical problem of motion artifacts. This device has proven its capacity to deliver

computer-controlled, stable and reliable complex airflow patterns, outside as well as inside the MRI scanner with an easy set-up.

Moreover, this device presents a vast modularity as demonstrated by the multiple stimuli used in this study, which could be even further increased by changing the positioning of the air puffs. Although the current device only has 4 air channels, it can easily be expanded to include other channels by adding more solenoid valves. This would allow further exploration of somatotopic maps of any part of the body, or to measure the effects of attention to specific complex stimuli (Puckett et al., 2017) or specific body sites of stimulation.

The airflow stimulator provides a set-up to explore tactile global flow processing with many possibilities to modulate individually the pneumatic channels and create numerous flow patterns adapted to the needs of the experimental designs. The fact that participants were able to finely discriminate patterns of stimulation varying in direction confirms that this device can be used to simulate complex dynamic stimuli. It offers the possibility to explore dynamic and not only static touch over any part of the body.

A noteworthy finding is that these different patterns of stimulation were found to be coded in specific brain regions, meaning that neural underpinnings of complex dynamic stimuli can be explored by a combination of the present device and an fMRI approach.

Finally, as this device can produce fine sensation of tactile flows, through complex spatio-temporal patterns, similar to visual optic flows, it also opens a new avenue to further explore the integrative mechanisms of multisensory motion signals.

## *ACKNOWLEDGEMENTS*

Funding: This work has received support from the French government under the Programme "Investissements d'Avenir", Initiative d'Excellence d'Aix-Marseille Université via AMidex funding (AMX-19-IET-004). JCG was funded by the *Agence Nationale de la Recherche* grant (nEURo*AMU, ANR-11- IDEX-0 0 01-02 grant). This work was performed in the Center IRM-INT@CERIMED (UMR 7289, AMU-CNRS), platform member of France Life Imaging network (grant ANR-11-INBS-0 0 06).

## *REFERENCES*


Abraham, A., Pedregosa, F., Eickenberg, M., Gervais, P., Mueller, A., Kossaifi, J., Varoquaux, G., 2014. Machine learning for neuroimaging with scikit-learn. Frontiers in neuroinformatics, 8, 14. https://doi.org/10.3389/fninf.2014.00014

Amemiya, T., Beck, B., Walsh, V., Gomi, H., Haggard, P., 2017. Visual area V5 / hMT + contributes to perception of tactile motion direction : a TMS study. Nat. Publ. Gr. 1–7. https://doi.org/10.1038/srep40937

Arnoldussen, D.M., Goossens, J., Van Den Berg, A. V., 2011. Adjacent visual representations of self-motion in different reference frames. Proc. Natl. Acad. Sci. U. S. A. 108, 11668–11673. https://doi.org/10.1073/pnas.1102984108

Basso, D., Pavan, A., Ricciardi, E., Pietrini, P., 2012. Touching Motion : rTMS on the Human Middle Temporal Complex Interferes with Tactile Speed Perception 389–398. https://doi.org/10.1007/s10548-012-0223-4

Behzadi Y, Restom K, Liau J, Liu TT, 2007. A component based noise correction method (CompCor) for BOLD and perfusion based fMRI. Neuroimage. 37(1):90-101. doi: 10.1016/j.neuroimage.2007.04.042.

Blake, R., Sobel, K. V., James, T.W., 2004. Neural synergy between kinetic vision and touch. Psychol. Sci. 15, 397–402. https://doi.org/10.1111/j.0956-7976.2004.00691.x

Cardillo, G., 2021. Jonckheere-Terpstra test on trend (https://github.com/dnafinder/jttrend), GitHub. Retrieved September 29, 2021.

Cheng, C. P., Halchenko, Y. O., 2020 A New Virtue of Phantom MRI Data: Explaining Variance in Human Participant Data. F1000Res, 9, 1131. https://doi.org/10.12688/f1000research.24544.1.

Debowska, W., Wolak, T., Soluch, P., Orzechowski, M., Kossut, M., 2013. Design and evaluation of an innovative MRI-compatible Braille stimulator with high spatial and temporal resolution. J. Neurosci. Methods 213, 32–38. https://doi.org/10.1016/j.jneumeth.2012.12.002

Dresel, C., Parzinger, A., Rimpau, C., Zimmer, C., Ceballos-Baumann, A.O., Haslinger, B., 2008. A new device for tactile stimulation during fMRI. Neuroimage 39, 1094–1103. https://doi.org/10.1016/j.neuroimage.2007.09.033

Esteban O., Birman D., Schaer M., Koyejo O.O., Poldrack R.A., Gorgolewski K.J., 2017. MRIQC: Advancing the automatic prediction of image quality in MRI from unseen sites. PLoS One. 12(9):e0184661. doi: 10.1371/journal.pone.0184661.

Esteban O., Markiewicz C.J., Blair R.W., Moodie C.A., Isik A.I., Erramuzpe A., Kent J.D., Goncalves M., DuPre E., Snyder M., Oya H., Ghosh S.S., Wright J., Durnez J., Poldrack R.A., Gorgolewski K.J., 2019. fMRIPrep: a robust preprocessing pipeline for functional MRI. Nat Methods. 16(1):111-116. doi: 10.1038/s41592-018-0235-4.

Feinberg D.A., Moeller S., Smith S.M., Auerbach E., Ramanna S., Gunther M., Glasser M.F., Miller K.L., Ugurbil K., Yacoub E., 2010. Multiplexed echo planar imaging for sub-second whole brain FMRI and fast diffusion imaging. PLoS One. 5(12):e15710. doi: 10.1371/journal.pone.0015710. Erratum in: PLoS One. 2011;6(9). doi: 10.1371/annotation/d9496d01-8c5d-4d24-8287-94449ada5064. Gunther, Matthias [added].

Fonov V.S., Evans A.C., McKinstry R.C., Almli C.R., Collins D.L., 2009 Unbiased nonlinear average age-

appropriate brain templates from birth to adulthood, NeuroImage. Volume 47, Supplement 1, Page S102, ISSN 1053-8119,https://doi.org/10.1016/S1053-8119(09)70884-5.

Friston K.J., Williams S., Howard R., Frackowiak R.S., Turner R., 1996. Movement-related effects in fMRI time-series. Magn Reson Med. 35(3):346-55. doi: 10.1002/mrm.1910350312.

Gorgolewski K., Burns C.D., Madison C., Clark D., Halchenko Y.O., Waskom M.L., Ghosh S.S., 2011. Nipype: a flexible, lightweight and extensible neuroimaging data processing framework in python. Front Neuroinform. 5:13. doi: 10.3389/fninf.2011.00013.

Gorgolewski K.J., Auer T., Calhoun V.D., Craddock R.C., Das S., Duff E.P., Flandin G., Ghosh S.S., Glatard T., Halchenko Y.O., Handwerker D.A., Hanke M., Keator D., Li X., Michael Z., Maumet C., Nichols B.N., Nichols T.E., Pellman J., Poline J.B., Rokem A., Schaefer G., Sochat V., Triplett W., Turner J.A., Varoquaux G., Poldrack R.A., 2016. The brain imaging data structure, a format for organizing and describing outputs of neuroimaging experiments. Sci Data. 3:160044. doi: 10.1038/sdata.2016.44.

Hao, Y., Manor, B., Liu, J., Zhang, K., Chai, Y., Lipsitz, L., Peng, C.K., Novak, V., Wang, X., Zhang, J., Fang, J., 2013. Novel MRI-compatible tactile stimulator for cortical mapping of foot sole pressure stimuli with fMRI. Magn. Reson. Med. 69, 1194–1199. https://doi.org/10.1002/mrm.24330

Huang, R.S., Sereno, M.I., 2007. Dodecapus: An MR-compatible system for somatosensory stimulation. Neuroimage 34, 1060–1073. https://doi.org/10.1016/j.neuroimage.2006.10.024

Indovina, I., Maffei, V., Pauwels, K., Macaluso, E., Orban, G.A., Lacquaniti, F., 2013. Simulated self-motion in a visual gravity field: Sensitivity to vertical and horizontal heading in the human brain. Neuroimage 71, 114–124. https://doi.org/10.1016/j.neuroimage.2013.01.005

Kleinschmidt, A., Thilo, K. V., Büchel, C., Gresty, M.A., Bronstein, A.M., Frackowiak, R.S.J., 2002. Neural correlates of visual-motion perception as object- or self-motion. Neuroimage 16, 873–882. https://doi.org/10.1006/nimg.2002.1181

Kovacs, G., Raabe, M., Greenlee, M.W., 2008. Neural Correlates of Visually Induced Self-Motion Illusion in Depth. https://doi.org/10.1093/cercor/bhm203

Landelle, C., El Ahmadi, A., Kavounoudias, A., 2018. Age-Related Impairment of Hand Movement Perception Based on Muscle Proprioception and Touch. Neuroscience. 381:91-104. https://doi: 10.1016/j.neuroscience.2018.04.015.

Landelle, C., Anton, J.L., Nazarian, B., Sein, J., Gharbi, A., Félician, O., Kavounoudias, A., 2020. Functional brain changes in the elderly for the perception of hand movements: a greater impairment in proprioception than touch. NeuroImage 17, 117056. https://doi: 10.1016/j.neuroimage.2020.117056

Moeller S., Yacoub E., Olman C.A., Auerbach E., Strupp J., Harel N., Uğurbil K., 2010. Multiband multislice GE-EPI at 7 tesla, with 16-fold acceleration using partial parallel imaging with application to high spatial and temporal whole-brain fMRI. Magn Reson Med. 63(5):1144-53. doi: 10.1002/mrm.22361.

Moulton, E.A., Pendse, G., Morris, S., Aiello-Lammens, M., Becerra, L., Borsook, D., 2009. Segmentally arranged somatotopy within the face representation of human primary somatosensory cortex. Hum. Brain Mapp. 30, 757–765. https://doi.org/10.1002/hbm.20541

Puckett A.M., Bollmann S., Barth M., Cunnington R., 2017. Measuring the effects of attention to individual fingertips in somatosensory cortex using ultra-high field (7T) fMRI. Neuroimage.

161:179-187. doi: 10.1016/j.neuroimage.2017.08.014. PMID: 28801252.

Ricciardi, E., Vanello, N., Sani, L., Gentili, C., Scilingo, E.P., Landini, L., Guazzelli, M., Bicchi, A., Haxby, J. V., Pietrini, P., 2007. The effect of visual experience on the development of functional architecture in hMT+. Cereb. Cortex 17, 2933–2939. https://doi.org/10.1093/cercor/bhm018

Sani, L., Ricciardi, E., Gentili, C., Vanello, N., Haxby, J. V., Pietrini, P., 2010. Effects of visual experience on the human MT + functional connectivity networks : an fMRI study of motion perception in sighted and congenitally blind individuals 4, 1–9. https://doi.org/10.3389/fnsys.2010.00159

Summers, I.R., Francis, S.T., Bowtell, R.W., McGlone, F.P., Clemence, M., 2009. A functional-magnetic-resonance-imaging investigation of cortical activation from moving vibrotactile stimuli on the fingertip. J. Acoust. Soc. Am. 125, 1033–1039. https://doi.org/10.1121/1.3056399

Van Kemenade, B.M., Seymour, K., Wacker, E., Spitzer, B., Blankenburg, F., Sterzer, P., 2014. Tactile and visual motion direction processing in hMT+/V5. Neuroimage 84, 420–427. https://doi.org/10.1016/j.neuroimage.2013.09.004

Wacker, E., Spitzer, B., Lützkendorf, R., Bernarding, J., Blankenburg, F., 2011. Tactile motion and pattern processing assessed with high-field fmRi. PLoS One 6. https://doi.org/10.1371/journal.pone.0024860

Xu J., Moeller S., Auerbach E.J., Strupp J., Smith S.M., Feinberg D.A., Yacoub E., Uğurbil K., 2013. Evaluation of slice accelerations using multiband echo planar imaging at 3 T. Neuroimage. 83:991-1001. doi: 10.1016/j.neuroimage.2013.07.055.

Yang, J., Wu, J., He, J., 2011 Programmable Tactile Pattern Presentations Operational under MRI to Investigate Neural Mechanisms of Tactile Shape Discrimination. Journal of Neuroscience Methods, 201 (1), 17–26. https://doi.org/10.1016/j.jneumeth.2011.06.030.

Zappe, A.C., Maucher, T., Meier, K., Scheiber, C., 2004. Evaluation of a Pneumatically Driven Tactile Stimulator Device for Vision Substitution during fMRI Studies. Magn. Reson. Med. 51, 828–834. https://doi.org/10.1002/mrm.20021

## *FIGURE LEGENDS*

**Figure 1. Schematic representation of the pneumatic components of the PAF device**
Pneumatic circuit diagram includingthree-stage circuit : A) pressure regulation stage in which the medical air source, which has a maximal pressure of 5 bars, is regulated by an electropneumatic pressure regulator which ensures the distribution of 2 bars to each downstream electrovalves, B) The flow distribution is modulated by proportional electrovalves and monitored using flowmeters, C) the air is transported via polyurethane hoses that are embedded in acetal copolymer hoses (blue) and nozzles (yellow), to reach the participant's body (in this study : the participant's face).

**Figure 2. Overview of the control on the PAF device**
A real-time software supervisor, written on LabVIEW © 2017, allows the online monitoring of the four pneumatic channels and control of the global airflow input rate. The solenoid valve opening is controlled using a specific electronic circuit converting the analog variable output voltage from the NI 6289 to a variable current that modulates the valve opening. A flowmeter device allows the visual control of the flow rates in each channel.

**Figure 3. The Airflow device and example of airflow spatial patterns.**
**A.** Air flow stimulator mounting device. The polyurethane hoses are plugged onto the acetal copolymer hoses (blue component) and nozzles (orange component) and constitute four air puffs (AP). This part of the setup is fixed onto a mounting device (white) that can be clipped-on the MRI scanner's bed. **B.** Three flow -levels were defined (LVL1, LVL2, LVL3) and each of the four air puffs (AP1, AP2, AP3, AP4) were individually calibrated. Each pattern was created to produce different global flow directions. The five patterns correspond to the five directions of the psychophysical experiment (from leftmost to rightmost). The fMRI run used different temporal sequences of these patterns.

**Figure 4. Behavioral results on the perception of direction of the airflow stimuli.**
**A.** Mean trackball responses for theLeftMost to the RightMost tactile stimuli. For each direction of stimulation, the mean trackball response per participant (one circle represents one participant's mean value) is plotted using a scale range from -10 to +10 (1 unit = 5.4°). **B.** Tactile psychophysical curves for one subject. Proportions of "right" answers are plotted as a function of the stimulus' direction from LeftMost (1 a.u.) to RighMost (5 a.u.). Perpendicular dashed lines represent the intensities corresponding to the 25% and 75% thresholds extracted to compute the discrimination threshold (JND).

**Figure 5.**
Visualization of one slice of the MPRAGE (top row) and EPI (bottom row) sequences when the device is out of the room (left column) and in close proximity of the headcoil and in function (right column) did not reveal any impact of the presence of the PAF device.

**Figure 6. Head movements and onsets of puff stimuli.**
**A-B.** Colored lines represent the mean head movements, over the 20 participants, in the translational components (in mm) **(A)** and rotational components (in rad) **(B)** for the three directions (x: green; y: blue; z: red). **C.** Mean framewise displacement (FD, in mm) calculated by FMRIPREP over all 20 participants. Each vertical line corresponds to the onset of a puff stimulus (Left, Right, Flicker, Motion or Target)

**Figure 7. Brain regions more activated during the Tactile Motion versus Static conditions (Tactile Motion > Flicker)**.
Cortical statistical map ($p < 0.05$ FWE cluster corrected) obtained in the group-analysis is overlaid on inflated brain cortical surface and sagittal slices of a mean normalized anatomical image (x coordinates in MNI space). *L: left hemisphere, R: right hemisphere, Cereb: cerebellum, IFG: inferior frontal gyrus, INS: Insula, SI: primary somatosensory area, SII: secondary somatosensory area, SMG: SupraMarginal Gyrus.*

**Figure 8. Group-level anatomical Region-of-Interest tactile decoding analysis.**
Violin plots represent the decoding accuracy of the four classes of tactile motion (Motion, Flicker, Left, Right) computed for 5 regions of interests (SI, SII, IPL, SPL, V1) in both hemispheres (L, R) for all participants. The horizontal black line represents the chance level (25%). Colored circles represent individual decoding accuracy, white circles and vertical black lines represent the population's median and standard deviation respectively. A right-tailed Wilcoxon signed rank test against chance level (25%) was performed. * : $p<0.05$, ** : $p<0.01$, *** : $p<0.001$.